BIOCHEMISTRY
including biophysical chemistry & molecular biology
Article

Biochemistry **2010,** *49,* 8105–8116 8105
DOI: 10.1021/bi100644q

Kinetic Analysis Reveals Differences in the Binding Mechanism of Calmodulin and Calmodulin-like Protein to the IQ Motifs of Myosin-10†

Ariel J. Caride, Richard D. Bennett,‡ and Emanuel E. Strehler*

Department of Biochemistry and Molecular Biology, Mayo Clinic College of Medicine, Rochester, Minnesota 55905
‡Present address: McLaughlin Research Institute, Great Falls, MT 59405.

Received April 26, 2010; Revised Manuscript Received August 18, 2010

ABSTRACT: Myo10 is an unconventional myosin with important functions in filopodial motility, cell migration, and cell adhesion. The neck region of Myo10 contains three IQ motifs that bind calmodulin (CaM) or the tissue-restricted calmodulin-like protein (CLP) as light chains. However, little is known about the mechanism of light chain binding to the IQ motifs in Myo10. Binding of CaM and CLP to each IQ motif was assessed by nondenaturing gel electrophoresis and by stopped-flow experiments using fluorescence-labeled CaM and CLP. Although the binding kinetics are different in each case, there are similarities in the mechanism of binding of CaM and CLP to IQ1 and IQ2: for both IQ motifs Ca^{2+} increased the binding affinity, mainly by increasing the rate of the forward steps. The general kinetic mechanism comprises a two-step process, which in some cases may involve the binding of a second IQ motif with lower affinity. For IQ3, however, the kinetics of CaM binding is very different from that of CLP. In both cases, binding in the absence of Ca^{2+} is poor, and addition of Ca^{2+} decreases the K_d to below 10 nM. However, while the CaM binding kinetics are complex and best fitted by a multistep model, binding of CLP is fitted by a relatively simple two-step model. The results show that, in keeping with growing structural evidence, complexes between CaM or CaM-like myosin light chains and IQ motifs are highly diverse and depend on the specific sequence of the particular IQ motif as well as the light chain.

Myosin-10 (Myo10)[1] is an unconventional myosin associated with dynamic actin remodeling and involved in filopodial extension, cell adhesion, and mitotic spindle orientation, among its multiple functions (*1*−*6*). The basic structure of Myo10 is common to unconventional myosins: the N-terminal head, which binds actin and displays actin-activated ATPase activity, is followed by a neck comprised of three light chain-binding IQ motifs and a tail, which in Myo10 includes a putative coiled-coil region, PEST motifs, three PH (pleckstrin homology) domains, a MyTH4 (myosin tail homology 4) domain that binds microtubules, and a FERM (band 4.1/ezrin/radixin/moesin) domain. The presence of MyTH4 and FERM domains relates this myosin with myosins of classes VII and XV involved in hereditary deafness and blindness syndromes (*7*, *8*).

The regulation of Myo10 by its light chains is poorly understood. As in most other unconventional myosins, calmodulin (CaM) is thought to be the principal light chain of Myo10 (*9*−*11*). In addition, however, the epithelial-specific calmodulin-like protein (CLP) also binds to Myo10 as a specific light chain (*12*), increasing Myo10 expression and stimulating the Myo10-dependent growth of filopodia (*13*). This raises questions as to how CaM and CLP bind to and compete for the individual IQ sites on Myo10. Because CLP differs from CaM in its Ca^{2+} binding characteristics (*14*), the effect of Ca^{2+} on the binding and occupancy of each IQ domain by CaM and CLP also remains unexplored.

There is virtually no information on the kinetic mechanism(s) by which CaM and CLP bind to the IQ motifs in the neck of Myo10. Indeed, little is known about the kinetics of binding of CaM (or CaM-like light chain) to any unconventional myosin. Moreover, how Ca^{2+} affects the mechanism of binding of either light chain to the IQ motifs in the neck of Myo10 is unknown. The purpose of this work was to start filling this void. We performed equilibrium and fast-kinetic experiments to elucidate the mechanism of binding of both CaM and CLP to each of the IQ motifs in Myo10. Our results show that while CaM and CLP bind with moderate affinity to the isolated IQ2 domain in the absence of Ca^{2+}, both light chains display dramatically increased affinity for each of the three IQ domains in the presence of Ca^{2+}. The studies further indicate different binding mechanisms for CLP and CaM to IQ3, suggesting structural differences between the CaM−IQ3 and CLP−IQ3 complexes.

EXPERIMENTAL PROCEDURES

Origin and Preparation of Reagents. CaM was purchased from Calbiochem (La Jolla, CA). CLP was expressed in *Escherichia coli* and purified as described (*15*, *16*). 2-Chloro-(amino-Lys75)-[6-[4-(*N*,*N*-diethylamino)phenyl]-1,3,5-triazin-4-yl]-CaM (TA-CaM) was synthesized and purified as described (*17*). Purity was confirmed as reported earlier (*18*). TA-CLP was

†This work was supported by the Mayo Clinic Cancer Center, the Mayo Foundation for Medical Research and Education, and the Mayo Graduate School (to R.D.B.).

*To whom correspondence should be addressed. Tel: (507) 284-9372. Fax: (507) 284-2384. E-mail: strehler.emanuel@mayo.edu.

[1]Abbreviations: CaM, calmodulin; CLP, calmodulin-like protein; EGTA, ethylene glycol bis(2-aminoethyl ether)-*N*,*N*,*N*′,*N*′-tetraacetic acid; FERM, band 4.1/ezrin/radixin/moesin; HPLC, high-pressure liquid chromatography; Myo10, myosin-10; MyTH4, myosin tail homology 4; PH, pleckstrin homology; TA, 2-chloro-(amino-Lys75)-[6-[4-(*N*,*N*-diethylamino)phenyl]-1,3,5-triazin-4-yl]; TEA, triethanolamine.

Published on Web 08/23/2010

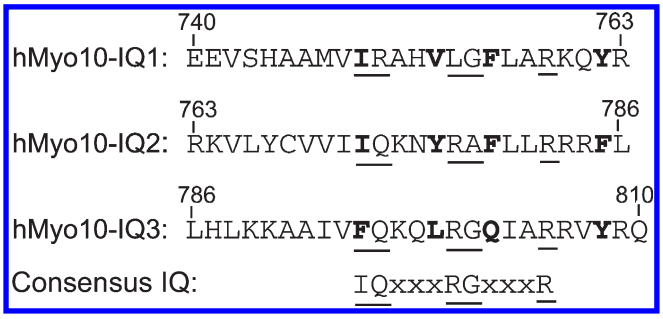

FIGURE 1: Sequence of the three IQ motifs in Myo10. The underlined residues are in the positions of the consensus IQ motif IQxxxRGxxxR, and the residues indicated in bold are the hydrophobic residues in positions 1−5−8−14. The first and last residues of each IQ peptide are numbered according to their position in full-length human Myo10.

synthesized the same way except that bacterially expressed and purified CLP was used as protein. TA-CaM and TA-CLP were kind gifts from Dr. Katalin Török (St. Geoge Hospital Medical School, London, U.K.) and Dr. Richard Thorogate (London Centre for Nanotechnology, University College London, U.K.).

Synthetic Peptides. Peptides corresponding to IQ motifs 1−3 were synthesized by the Mayo Peptide Core Facility and purified to homogeneity by HPLC. A second batch of IQ3 peptide was synthesized and purified by Anaspec, Inc. (San Jose, CA). The sequences of the peptides are shown in Figure 1.

Protein−Peptide Complex Formation and Nondenaturing Electrophoresis. Aliquots of purified CaM or CLP (10 μg, 0.6 nmol) were mixed with equimolar amounts of IQ1, IQ2, or IQ3 peptide in a final volume of 20 μL sample buffer (25 mM Tris-HCl, pH 6.8, 10% glycerol, 0.1 mM $CaCl_2$) and incubated at room temperature for 15 min. For competition experiments, equimolar amounts of CLP and CaM were added to the samples containing the preformed CaM−IQ and CLP−IQ complexes, respectively, and incubated for an additional 15 min. Nondenaturing electrophoresis was performed in 10% polyacrylamide gels in 25 mM Tris−glycine (pH 8.3) and 100 μM $CaCl_2$. After running, the gels were stained with Coomassie Brilliant Blue.

Equilibrium Fluorescence. Equilibrium binding of IQ peptides to TA-CaM and TA-CLP was measured at 25 °C in a Varian Cary Eclipse spectrofluorometer. Measurements were made in media containing 120 mM KCl, 30 mM Tes−triethanolamine (Tes−TEA, pH 7.2), 5 mM $MgCl_2$, 5 mM NaN_3, and 10 mM EGTA (absence of Ca^{2+}) or 0.2 mM EGTA and enough $CaCl_2$ to obtain 100 μM free Ca^{2+} (presence of Ca^{2+}). The concentration of either TA-CaM or TA-CLP was 34 nM. The excitation wavelength was 370 nm, and the emission wavelength was 420 nm.

Stopped-Flow Rapid Mixing Experiments. Stopped-flow measurements of changes in fluorescence of TA-CaM or TA-CLP were performed in an Applied Photophysics SX.18MV reaction analyzer at 25 °C. The excitation wavelength was 365 nm, and the emitted light was detected using a 390 nm cutoff filter. The final mix contained 17 nM TA-CaM or TA-CLP and the concentration of IQ peptides indicated in the legend of the figures, in buffer containing 30 mM Tes−TEA (pH 7.2), 120 mM KCl, 5 mM $MgCl_2$, 0.2 mM EGTA, and enough $CaCl_2$ to obtain 100 μM free Ca^{2+} (or 10 mM EGTA for measurements in the absence of Ca^{2+}). For experiments in the presence of Ca^{2+}, $CaCl_2$ was included in both syringes.

Analysis of Results and Modeling. Preliminary analysis of the fluorescence traces was performed by fitting mono- or multiexponential functions to the data. This was done to obtain an approximate idea of whether a single-step or multistep kinetic model might be appropriate. Fitting to specific kinetic models was then performed by global nonlinear regression analysis using the Dynafit software (www.biokin.com). Global analysis refers to the fact that all progress curves are fitted at once rather than individually. This allows greater discriminatory power between models and enhanced accuracy in determining the kinetic parameters. The software allows direct fitting of predetermined kinetic models to experimental data. The differential equations derived from the kinetic models are solved numerically rather than analytically. In this way, several models of different complexity can be easily tested. When the choice of the best model was not obvious, kinetic models were chosen on the basis of Akaike information criteria (*19*). These are based on information theory and statistical methods and take into account the number of parameters as well as the differences between the model and data χ^2 (weighted sum of least-squares differences). Thus, the tighter fitting for models with a larger number of parameters is balanced against the requirement to use the minimal number of parameters for the fit, with a penalty imposed for the total number of parameters. We have used this procedure before with great success to analyze kinetic data of the binding of peptides corresponding to the calmodulin-regulated domain of the calcium pump to calmodulin (*18*, *20*).

RESULTS

CLP and CaM Bind to Each IQ Motif of Myo10, and CLP Effectively Competes with CaM for IQ Binding. Figure 1 shows the sequence of the three IQ motifs in Myo10. Although the main conserved sequence features of an IQ motif are recognizable in each of these motifs, there are substantial variations and substitutions compared to the consensus sequence IQxxxRGxxxR. For example, in IQ1 the canonical Q is replaced by R, and the first canonical R is replaced by L. Likewise, in IQ2 the G is replaced by an A, and in IQ3, the I is replaced by a bulkier F. In view of the different characteristics of these motifs, we studied the binding of the two known light chains of Myo10, CaM and CLP, to the isolated IQ motifs in more detail.

To qualitatively verify the binding of the IQ peptides to each of the light chains, we first mixed IQ peptides and CaM or CLP in stoichiometric amounts in a Ca^{2+}-containing buffer and observed the complexes formed by nondenaturing electrophoresis. It should be noted that under these conditions differences in the mobility of the bands on the gel mainly reflect differences in charge and shape, rather than in size, of the protein−IQ peptide complexes. The results are shown in Figure 2. In panel A, each sample contained an equal amount of CaM. Lane 1 shows CaM alone. Lane 2 contained CaM and CLP mixed in equal amounts, demonstrating that CaM and CLP are easily distinguishable in these native gels. Lane 3 shows an equimolar mixture of IQ1 peptide and CaM. The double band indicates the presence of both free CaM and the CaM−IQ1 peptide complex (labeled a in Figure 2). Adding an equimolar amount of CLP to the CaM−IQ1 sample results in the formation of the CLP−IQ1 complex (broad band labeled b in lane 4) and a decrease in the band corresponding to the IQ1−CaM complex. Similarly, lane 5 shows that mixing CaM and IQ2 leads to the virtually quantitative formation of the IQ2−CaM complex (labeled c). When CLP is added, the band corresponding to the IQ2−CaM complex is no longer visible, and a new band of lesser mobility is formed along with the reappearance of the band for free CaM (lane 6). The new band (labeled d) corresponds to the CLP−IQ2 complex. Lastly, when IQ3 is

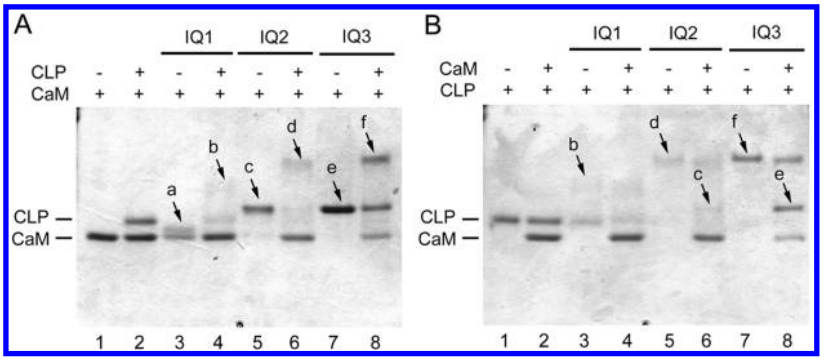

FIGURE 2: Identification of CaM−IQ and CLP−IQ complexes by nondenaturing gel electrophoresis. Complexes were formed, and the gels were run as described in the Experimental Procedures. In panel A, all lanes contained 10 μg of CaM. Lanes 2, 4, 6, and 8 also contained 10 μg of CLP. Lanes 3 and 4 contained an amount of IQ1 equimolar with the amount of CaM, lanes 5 and 6 contained equimolar amounts of IQ2, and lanes 7 and 8 contained equimolar amounts of IQ3. In panel B, all lanes contained 10 μg of CLP, lanes 2, 4, 6, and 8 also contained 10 μg of CaM, lanes 3 and 4 contained IQ1, lanes 5 and 6 contained IQ2, and lanes 7 and 8 contained IQ3, all in equimolar amounts.

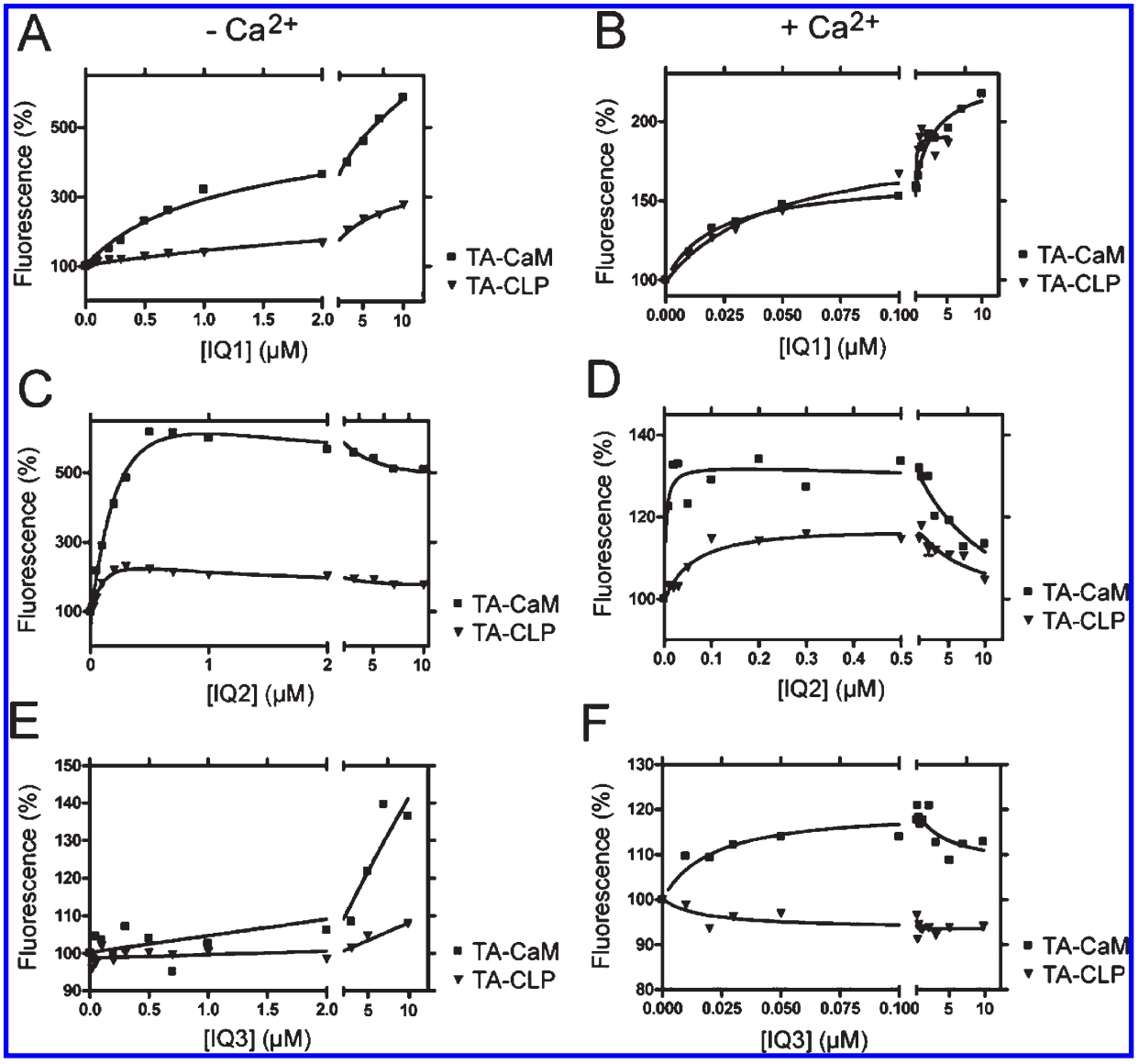

FIGURE 3: Titration of TA-CaM and TA-CLP with the IQ motifs of Myo10, in the absence (A, C, and E) and in the presence (B, D, and F) of Ca^{2+}. Titrations were done by monitoring the fluorescence of TA-CaM or TA-CLP at 25 °C in the media described in the Experimental Procedures. When the measurements were done in the absence of Ca^{2+}, the buffer contained 10 mM EGTA. When the measurements were done in the presence of Ca^{2+}, the buffer contained 0.2 mM EGTA and enough $CaCl_2$ to obtain 100 μM free Ca^{2+}. In each case, fluorescence is represented as a percentage of the fluorescence of the sample in the absence of IQ peptide.

added to CaM (lane 7), the presence of a band of lesser mobility, together with the disappearance of the band corresponding to free CaM, indicates the formation of the CaM−IQ3 complex (labeled e). Addition of CLP (lane 8) promotes the formation of

a new band of even lesser mobility, corresponding to the IQ3−CLP complex (labeled f), together with the reappearance of the band corresponding to free CaM. These results show that while CaM forms a complex with each of the three IQ peptides, CLP effectively competes with CaM for IQ binding, especially for binding to IQ2 and IQ3.

Figure 2B shows the reciprocal experiment where all samples contained an equal amount of CLP. Lane 1 shows the band corresponding to CLP alone, and lane 2 shows the bands corresponding to CLP and CaM. In lane 3, the complex (b) between CLP and IQ1 is seen as slowly migrating, diffuse band. This lane also shows a band corresponding to remaining free CLP, indicating that the CLP−IQ1 complex is not very stable under the conditions of the gel electrophoresis. Addition of CaM (lane 4) does not lead to a significant decrease in the amount of IQ1−CLP complex. Thus, the amount of IQ1−CaM complex formed appears to be small in the presence of CLP. Lane 5 shows the complex (d) between IQ2 and CLP. Addition of CaM (lane 6) results in the formation of some CaM−IQ2 complex (c), but there is little free CLP, indicating that CaM does not very effectively compete with CLP bound to IQ2. Similar results were obtained for the CLP−IQ3 complex (f), as shown in lanes 7 and 8 of panel B. Taken together, the results show that, at least in the presence of Ca^{2+}, complexes between the IQ peptides and CaM or CLP are formed and are stable enough to be visualized by nondenaturing gel electrophoresis. Furthermore, at least in the case of IQ2 and IQ3, CLP can effectively compete with CaM for the IQ motifs in Myo10 whereas CaM appears to be less effective in competing with CLP bound to these IQ peptides.

Quantitative Analysis of Binding of CLP and CaM to IQ 1, 2, and 3 of Myo10. To obtain quantitative measurements of CaM and CLP binding to the individual IQ motifs in Myo10, we performed binding experiments using fluorescence-labeled TA-CaM and TA-CLP. The advantage of labeling CaM or CLP with the TA fluorescent group is that the fluorescence is very sensitive to the environment, creating the opportunity to detect different steps during the binding process. This approach has previously been used with success to study the kinetic mechanism of the binding of CaM to the plasma membrane Ca^{2+} pump (*18*, *21*). Figure 3 shows the results of titrations of TA-CaM and TA-CLP with the IQ peptides in both the presence and absence of Ca^{2+}. In the absence of Ca^{2+}, binding of IQ1 to TA-CaM and TA-CLP increases the fluorescence of the labeled proteins about 6-fold in the case of TA-CaM and 3-fold in the case of TA-CLP (Figure 3A). The affinity of the interaction in the absence of Ca^{2+} is low (see Table 1), both for TA-CaM and TA-CLP. In the presence of 100 μM free Ca^{2+} the increase in TA-CaM and TA-CLP fluorescence upon IQ1 binding is smaller (about 2-fold for both TA-CaM and TA-CLP; Figure 3B). The shape of the curve is similar for IQ1 binding to TA-CaM and TA-CLP. It shows a high-affinity component and a smaller, low-affinity increase in fluorescence. In Table 1 we report the K_d values of the high-affinity component. The data clearly show that Ca^{2+} promotes a large increase in the affinity of binding of IQ1 to both TA-CaM and TA-CLP.

The binding of IQ2 to TA-CaM and TA-CLP in the absence of Ca^{2+} results in an increase in the fluorescence of both proteins, followed by a small decrease in fluorescence at higher IQ2 concentrations (Figure 3C). The low-affinity components (at high peptide concentrations) in the titration curves for IQ1 and IQ2, although small, are important when interpreting the results of rapid kinetic experiments (see below). Ca^{2+} produces an increase in the affinity of both CaM and CLP for IQ2. As observed for IQ1, the change in fluorescence upon binding of IQ2 is much smaller in the presence of 100 μM Ca^{2+} (Figure 3D). Table 1 shows that the affinity of IQ2 for TA-CaM and TA-CLP is comparable, although CaM appears to bind IQ2 more strongly than CLP in the presence of Ca^{2+}.

Table 1: Parameters of TA-CaM and TA-CLP Binding to Myo10 IQ Peptides[a]

protein	condition[b]	K_d(IQ1) (nM)	K_d(IQ2) (nM)	K_d(IQ3) (nM)
CaM	$-Ca^{2+}$	5078 ± 1888	708 ± 48	> 50000
	$+Ca^{2+}$	152 ± 78	6.9 ± 6.1	9.4 ± 3.1
CLP	$-Ca^{2+}$	4938 ± 338	134 ± 27	NM[c]
	$+Ca^{2+}$	57 ± 35	46 ± 7	7.2 ± 4.4

[a]Equilibrium titrations were performed as described in the Experimental Procedures. Affinities for the high-affinity binding sites were determined from the binding isotherms and are reported as K_d values. [b]The buffer for the Ca^{2+}-free ($-Ca^{2+}$) condition contained 10 mM EGTA, whereas 100 μM Ca^{2+} was present in the Ca^{2+}-containing ($+Ca^{2+}$) condition. [c]Not measurable.

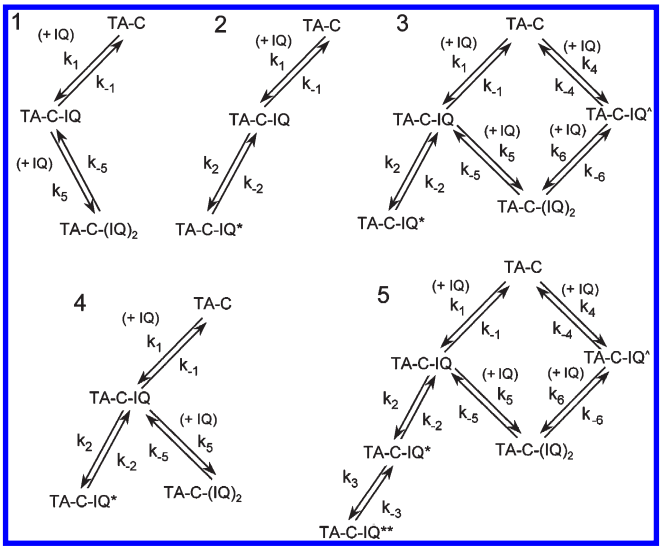

FIGURE 4: Schematic representation of the kinetic models used for fitting the data obtained in the stopped-flow experiments described in Figures 5−9. TA-C stands for either TA-CaM or TA-CLP. TA-C−IQ*, TA-C−IQ**, and TA-C−IQ^ denote different conformations of the complex of TA-CaM or TA-CLP with IQ peptide.

Panels E and F of Figure 3 show the effect of IQ3 binding to TA-CaM and TA-CLP in the absence and presence of Ca^{2+}, respectively. IQ3 binds with very low affinity to TA-CaM and TA-CLP in the absence of Ca^{2+} (Figure 3E). In the presence of Ca^{2+}, however, IQ3 binds to both proteins with very high affinity (Figure 3F and see Table 1). A comparison of the fluorescence curves in Figure 3F shows that while binding of IQ3 to TA-CaM produces an increase in fluorescence, binding to TA-CLP produces a small but significant *decrease* in fluorescence, suggesting a difference in the mechanism of binding of IQ3 to these proteins. This is different from the results obtained with IQ1 and IQ2, where binding of these peptides to both TA-CaM and TA-CLP produces similar changes in fluorescence.

Kinetic Analysis of TA-CaM and TA-CLP Binding to IQ1, IQ2, and IQ3. To study the mechanism of binding of CaM and CLP to the IQ motifs in Myo10, we performed stopped-flow experiments mixing TA-CaM or TA-CLP with peptides IQ1, IQ2, and IQ3, in the absence and in the presence of Ca^{2+}. To interpret these experiments, we considered for each reaction several kinetic models. The models were fitted to the experimental

Table 2: Kinetic Parameters for Binding of TA-CaM and TA-CLP to IQ Motifs in Myo10[a]

	TA-CaM					TA-CLP				
	IQ1		IQ2		IQ3	IQ1		IQ2		IQ3
	$-Ca^{2+}$ (model 1)	$+Ca^{2+}$ (model 4)	$-Ca^{2+}$ (model 4)	$+Ca^{2+}$ (model 4)	$+Ca^{2+}$ (model 5)	$-Ca^{2+}$ (model 1)	$+Ca^{2+}$ (model 3)	$-Ca^{2+}$ (model 4)	$+Ca^{2+}$ (model 4)	$+Ca^{2+}$ (model 2)
k_1 (μM^{-1} s^{-1})	0.662 ± 0.044	173.4 ± 1.1	78.74 ± 33.35	11.81 ± 1.536	450.2 ± 65.18	1.03 ± 0.048	4.24 ± 1.65	4.9719 ± 0.2134	52.14 ± 17.51	103.43 ± 5.857
k_{-1} (s^{-1})	8.423 ± 0.346	7.128 ± 0.125	12.503 ± 0.7889	27.187 ± 0.8348	118.04 ± 7.249	8.03 ± 0.2	7.50 ± 1.31	5.6748 ± 0.2905	29.03 ± 18.07	2.54 ± 0.6693
k_2 (s^{-1})		0.3153 ± 0.1174	7.5534 ± 0.6942	0.4685 ± 0.3594	2.072 ± 2.847		4.861 ± 3.026	2.9254 ± 0.2536	5.137 ± 3.794	2.166 ± 0.8612
k_{-2} (s^{-1})		3.8825 ± 0.2155	1.471 ± 0.1936	2.9365 ± 0.2101	4.215 ± 4.782		0.808 ± 0.2353	0.35875 ± 0.02875	1.157 ± 0.05252	0.015[b]
k_3 (s^{-1})					1.066 ± 1.868					
k_{-3} (s^{-1})					3.283 ± 3.466					
k_4 (μM^{-1} s^{-1})					406.98 ± 34.3		12.915 ± 1.221			
k_{-4} (s^{-1})					8.5281 ± 0.3125		2.0773 ± 0.1243			
k_5 (μM^{-1} s^{-1})	0.0941 ± 0.0148	90.21 ± 9.54	3.196 ± 1.696	31.651 ± 0.8853	< 0.0001	0.231 ± 0.017	0.4284 ± 0.6298	0.2129 ± 0.05354	27.93 ± 29.4	
k_{-5} (s^{-1})	3.036 ± 0.079	68.251 ± 5.44	1.175 ± 0.1493	14.027 ± 0.6736	165.9 ± 78.83	1.091 ± 0.022	3.526 ± 2.9	0.30602 ± 0.02266	5.989 ± 0.7487	
k_6 (μM^{-1} s^{-1})					6.755 ± 1.608		0.3229 ± 0.2473			
k_{-6} (s^{-1})					< 0.0005		< 0.0001			
$r_{TA\text{-}C}$	1	1	1	1	1	1	1	1	1	1
$r_{TA\text{-}C-IQ}$	1.41	2.33	1.466	4.336	1.538	2.14	1.939	2.19	1.11	0.935
$r_{TA\text{-}C-IQ2}$	1.88	1.61	3.89	1.449	0.273	2.40	4.694	0.98	1.19	
$r_{TA\text{-}C-IQ^{\wedge}}$					1.223		1.290			
$r_{TA\text{-}C-IQ^{*}}$		4.69	1.041	6.849	1.341		1.960	9.04	1.31	0.878
$r_{TA\text{-}C-IQ^{**}}$					2.768					

[a] k_x refers to the forward rate constants for each of the steps in the models considered, k_{-x} refers to the reverse rate constants, $r_{TA\text{-}x}$ refers to the relative fluorescence of the species considered, taking the fluorescence of TA-C as 1. [b] Estimated value as data noise prevented detailed model analysis.

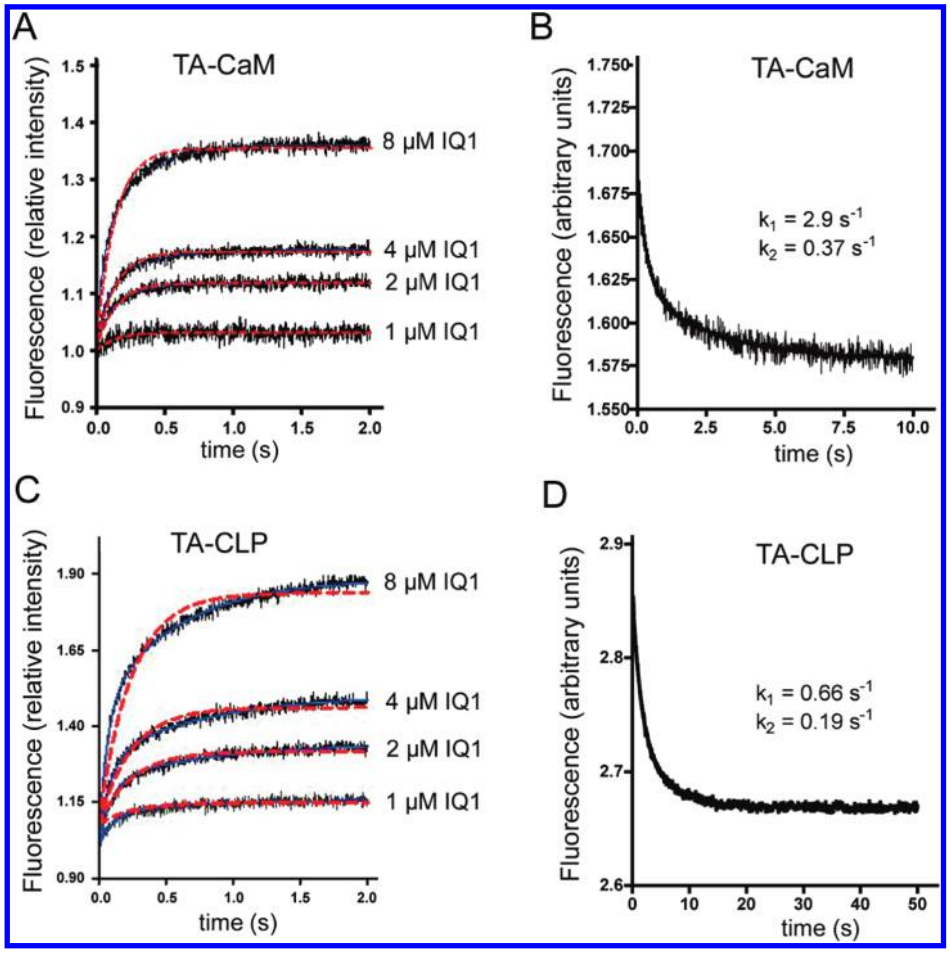

FIGURE 5: Kinetics of binding of TA-CaM and TA-CLP to IQ1 in the absence of Ca^{2+}. (A, C) Time course of fluorescence changes upon mixing 17 nM TA-CaM (A) or 17 nM TA-CLP (C) with the indicated concentrations of IQ1. The experimental data were best fitted (continuous blue line) with the model and kinetic constants shown in Table 2. For comparison, the fit using the simpler one-step model is also shown as a stippled red line, clearly indicating a poorer fit especially at higher IQ1 concentrations. (B, D) Progress curves of the dissociation of TA-CaM (B) or TA-CLP (D) from IQ1. 34 nM TA-CaM or 34 nM TA-CLP was premixed with 2 μM IQ1, and dissociation was initiated by adding 10 μM CaM (B) or 10 μM CLP (D). The progress curves were fitted with a sum of two exponentials, yielding the constants shown in the figure. All media contained 10 mM EGTA. In all cases, the indicated concentrations are after final mixing.

data by means of the Dynafit software (www.biokin.com). This approach has the advantage that the fitting is directly done by numerical integration based on the chemical equations involved rather than on exponential approximations. Figures 5−9 show the results of association and dissociation experiments of TA-CaM and TA-CLP with the different IQ peptides in the absence and in the presence of Ca^{2+}. The kinetic models used to fit the results are presented in Figure 4. Table 2 lists the model chosen and the values of the relevant constants obtained in each case. These will be discussed later to provide a comparative interpretation.

(*i*) *Binding to IQ1*. Figure 5A shows an experiment in which 17 nM TA-CaM was mixed with increasing concentrations of IQ1 (from 1 to 8 μM) in the absence of Ca^{2+}, and the fluorescence was recorded over time. This shows that binding of IQ1 to TA-CaM increases the fluorescence and that the increase in fluorescence is complete in about 0.5 s. Panel B shows the decrease in fluorescence when IQ1 dissociates from TA-CaM. Dissociation proceeds in a biphasic fashion with a fast phase ($k_1 = 2.9\ s^{-1}$) and a slower one ($k_2 = 0.37\ s^{-1}$).

Figure 5C shows the corresponding experiment where 17 nM TA-CLP was mixed with increasing concentrations of IQ1 (from 1 to 8 μM) in the absence of Ca^{2+}. As observed with TA-CaM, the binding of IQ1 to TA-CLP increases the fluorescence, and the increase in fluorescence is complete in about 2 s. Figure 5D shows the decrease in fluorescence when IQ1 dissociates from TA-CLP. Dissociation proceeds in a biphasic fashion with a faster ($k_1 = 0.66\ s^{-1}$) and a slower phase ($k_2 = 0.19\ s^{-1}$). For both TA-CaM and TA-CLP, model 1 (see Figure 4 and Table 2) provides an excellent fit to the data. The model indicates that TA-CaM (or TA-CLP) initially binds a single molecule of IQ1 and then is able to bind a second molecule, with lower affinity. For comparison, we also show in Figure 5A,C the fits (stippled red lines) obtained when a simpler one-step binding model was assumed for the IQ1 interaction with TA-CaM (or TA-CLP). This clearly shows that the simple model is inadequate to fit the data, especially at the higher peptide concentrations. Taken together, the results indicate that the kinetic mechanism of IQ1 binding to CaM and CLP in the absence of Ca^{2+} is essentially the same.

Figure 6 shows the kinetic analysis of the interaction of TA-CaM and TA-CLP with IQ1 in the presence of Ca^{2+}. The progress curves in Figure 6A were recorded upon mixing of 17 nM TA-CaM with different concentrations of IQ1 (from 0.1 to 0.8 μM) in the presence of 100 μM Ca^{2+}. The reaction was faster than in the absence of Ca^{2+}. In preliminary fittings, two exponential functions were needed to fit the experimental data, suggesting a multistep reaction. The time course of the dissociation of IQ1 from TA-CaM in the presence of 100 μM Ca^{2+} is shown in Figure 6B. Again the dissociation was biphasic with a faster ($k_1 = 2.5\ s^{-1}$) and

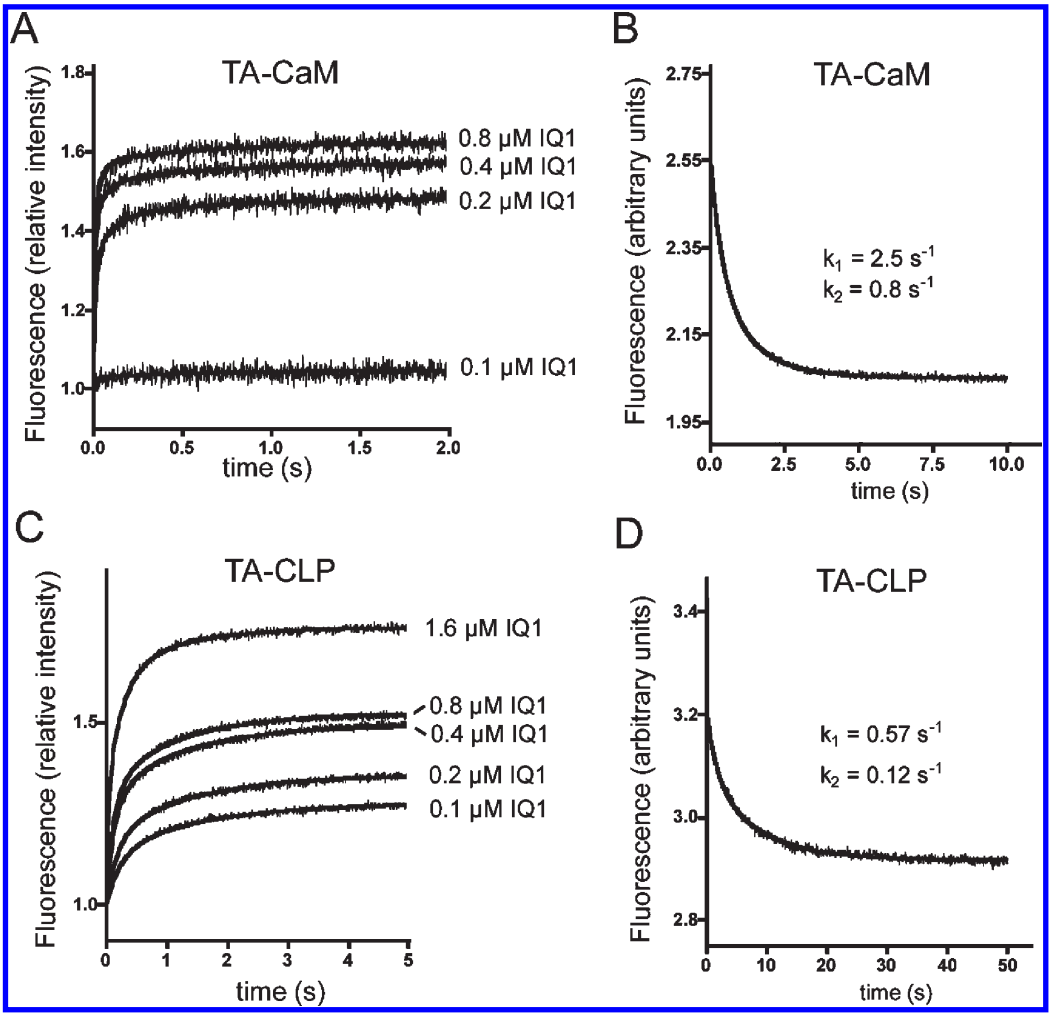

FIGURE 6: Kinetics of binding of TA-CaM and TA-CLP to IQ1 in the presence of 100 μM free Ca^{2+}. (A, C) Time course of fluorescence changes upon mixing 17 nM TA-CaM (A) or 17 nM TA-CLP (C) with the indicated concentrations of IQ1. The experimental data were fitted with the models and kinetic constants shown in Table 2. (B, D) Progress curves of the dissociation of TA-CaM (B) or TA-CLP (D) from IQ1. 34 nM TA-CaM or 34 nM TA-CLP was premixed with 0.2 μM IQ1, and dissociation was started by adding 1 μM CaM (B) or 1 μM CLP (D). The progress curves were fitted with a sum of two exponentials, with the constants shown in the figure. All media contained 0.2 mM EGTA and enough $CaCl_2$ to obtain 100 μM Ca^{2+}. In all cases, the indicated concentrations are after final mixing.

a slower (k_2 = 0.8 s^{-1}) component. The model required to fit the experimental results was more complex than that for fitting the data in the absence of Ca^{2+} and corresponds to model 4 in Figure 4. After binding a first IQ1 peptide, CaM may either undergo a subsequent conformational change (to yield the TA-CaM−IQ1* state), or it may bind a second IQ1 in no preferred order of addition.

The association and dissociation data for the interaction of TA-CLP with IQ1 in the presence of 100 μM Ca^{2+} are shown in Figure 6C,D. Both the association and the dissociation were slower than in the case of TA-CaM. However, the model used to fit the data is similar to that for binding of IQ1 to TA-CaM in the presence of Ca^{2+} (model 4), except that the binding of the second molecule of IQ1 does not occur until the first one is bound. The model is illustrated in Figure 4 as model 3.

(*ii*) *Binding to IQ2*. The results of the progress curves when 17 nM TA-CaM or TA-CLP was mixed with different concentrations of IQ2 in the absence of Ca^{2+} are shown in panels A and C of Figure 7, respectively. For both proteins, the association appears to have two phases, with a faster increase in fluorescence followed by a slower phase. This is more apparent at higher concentrations of IQ2. Panels B and D of Figure 7 show the kinetics of dissociation of IQ2 from TA-CaM and TA-CLP, respectively, in the same (Ca^{2+}-free) conditions. Again, the dissociation is biphasic with a fast component (k_1 = 0.34 s^{-1} for TA-CaM and 0.13 s^{-1} for TA-CLP) and a slower one (k_2 = 0.036 s^{-1} and 0.023 s^{-1}, respectively, for TA-CAM and TA-CLP). The model that gave the best fit of these data corresponds to model 4 in Figure 4. According to this model TA-CaM and TA-CLP bind one molecule of IQ2 and then can either undergo a conformational stabilization step or bind a second molecule of IQ2. Although the same model fitted the data for TA-CLP, the overall reaction for both association and dissociation was slower for TA-CLP than for TA-CaM (compare Figure 7, panels A and B with panels C and D).

Figure 8A,C shows the corresponding association data when 17 nM TA-CaM or TA-CLP was mixed with different concentrations of IQ2 in the presence of 100 μM Ca^{2+}. The results resemble those obtained in the absence of Ca^{2+}, except that the reaction is faster and we used lower concentrations of IQ2 peptide because of the higher affinity of TA-CaM and TA-CLP for IQ2 in Ca^{2+} conditions (see Table 1 and Figure 3). The dissociation reaction (Figure 8B,D) is also biphasic, although significantly slower than the same reaction in the absence of Ca^{2+} (compare Figure 8B with Figure 7B and Figure 8D with Figure 7D). The kinetic model used for the binding of IQ2 to TA-CaM and TA-CLP in the absence

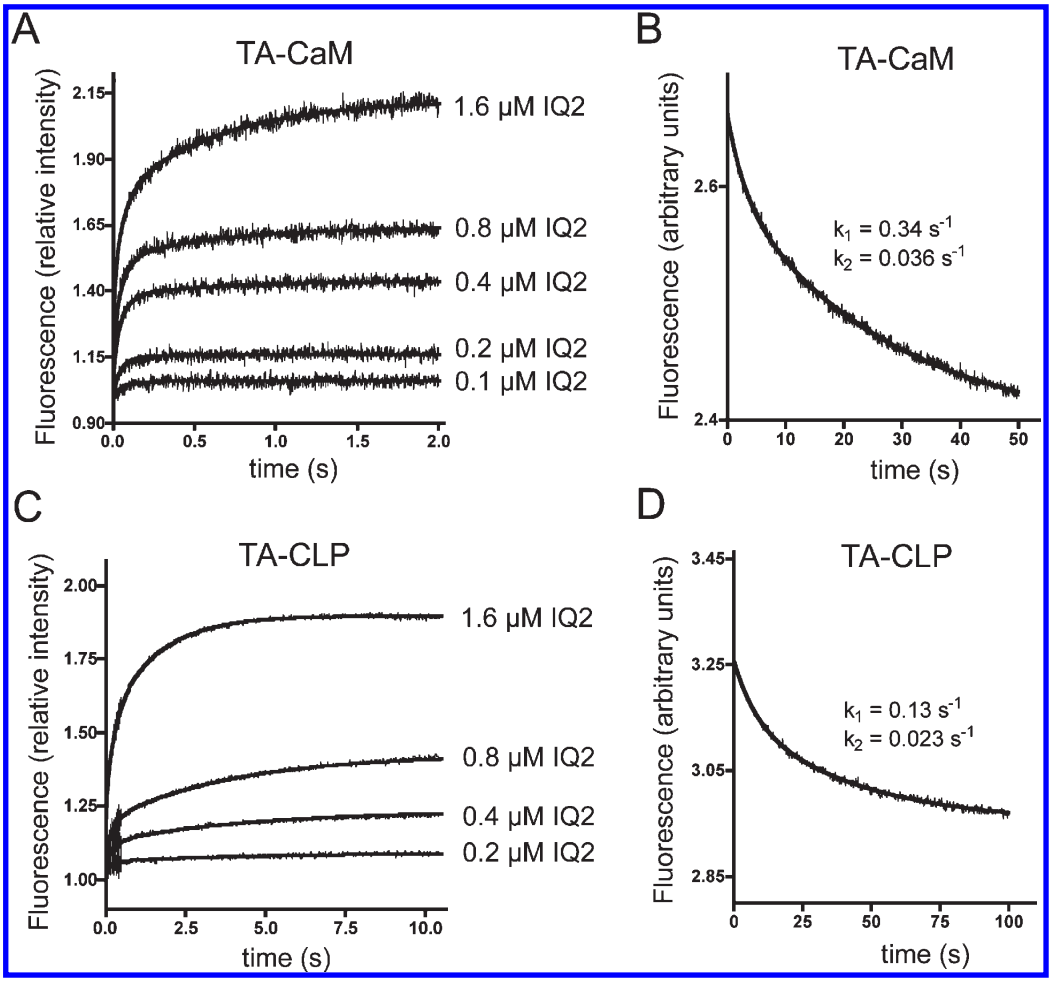

FIGURE 7: Kinetics of binding of TA-CaM and TA-CLP to IQ2 in the absence of Ca^{2+}. (A, C) Time course of fluorescence changes upon mixing 17 nM TA-CaM (A) or 17 nM TA-CLP (C) with the indicated concentrations of IQ2. The experimental data were fitted (smooth black lines) with the models and kinetic constants shown in Table 2. (B, D) Progress curves of the dissociation of TA-CaM (B) or TA-CLP (D) from IQ2. 34 nM TA-CaM or 34 nM TA-CLP was premixed with 0.2 μM IQ2, and dissociation was initiated by adding 1 μM CaM (B) or 1 μM CLP (D). The progress curves were fitted with a sum of two exponentials, with the rate constants shown in the figure. All media contained 10 mM EGTA. In all cases, the indicated concentrations are after final mixing.

of Ca^{2+} was equally able to fit the data in the presence of Ca^{2+} (model 4, Figure 4).

(*iii*) *Binding to IQ3*. We did not analyze the kinetics of binding of TA-CaM and TA-CLP to IQ3 in the absence of Ca^{2+} because the interaction is so weak that the data were not reliable (see also Figure 3 and Table 1). Therefore, the experiments on the kinetics of binding of IQ3 to TA-CaM and TA-CLP were performed only in the presence of 100 μM Ca^{2+}. In Figure 9A we show the changes in fluorescence when 17 nM TA-CaM was mixed with increasing concentrations of IQ3 from 0.05 to 2 μM. The fluorescence changes produced by IQ3 binding are very complex. At lower IQ3 concentrations, binding produces a small increase in fluorescence that follows approximately monoexponential kinetics. However, at higher IQ3 concentrations the progress curves show an increase, a decrease, and, at longer times, a new increase. At the highest IQ3 concentrations, the initial increase is so fast that it happens mostly during the dead time of the instrument (~1.3 ms). The dissociation curve is complex as well (Figure 9B). It shows an extremely rapid increase in fluorescence, a pronounced decrease, and a slow increase. These patterns indicate a multistep reaction pathway for both the association and the dissociation of IQ3 to and from TA-CaM. The model that best fit the experimental data corresponds to model 5 in Figure 4. It includes the possibility of the addition of a second IQ3 molecule, as well as two stabilization steps. Several models of lesser or similar complexity were tried but were unable to fit the data equally well.

In contrast to the complex behavior of TA-CaM, binding of 17 nM TA-CLP to IQ3 leads to a small decrease in fluorescence (Figure 9C) along a curve that could be fitted by the sum of two exponential functions. We assayed several concentrations of IQ3 from 0.1 to 1.6 μM, but for the sake of clarity only the extreme low and high concentrations are shown. Figure 9D shows the changes in fluorescence upon dissociation of IQ3 from TA-CLP. This shows a relatively slow (k = 0.015 s^{-1}) increase in fluorescence. The small total changes in fluorescence, and consequently the relatively larger noise in the data, prevented in this case a sophisticated model analysis, but model 2 in Figure 4 fit the results well. In this model, IQ3 binds to TA-CLP, and initial binding is followed by a second step resulting in an altered conformational state of the complex. Another model, in which IQ3 can bind to two alternative conformations of TA-CLP, was also able to fit the experimental data, but the Akaike information criteria were slightly better for model 2. Regardless of the actual model that is used to fit the data, it is clear that TA-CLP binds to IQ3 in a different manner than TA-CaM. This is a unique characteristic of the IQ3 motif, since in the case of IQ1 and IQ2 the models that fitted the binding progress curves were identical, or very similar, for TA-CaM and TA-CLP.

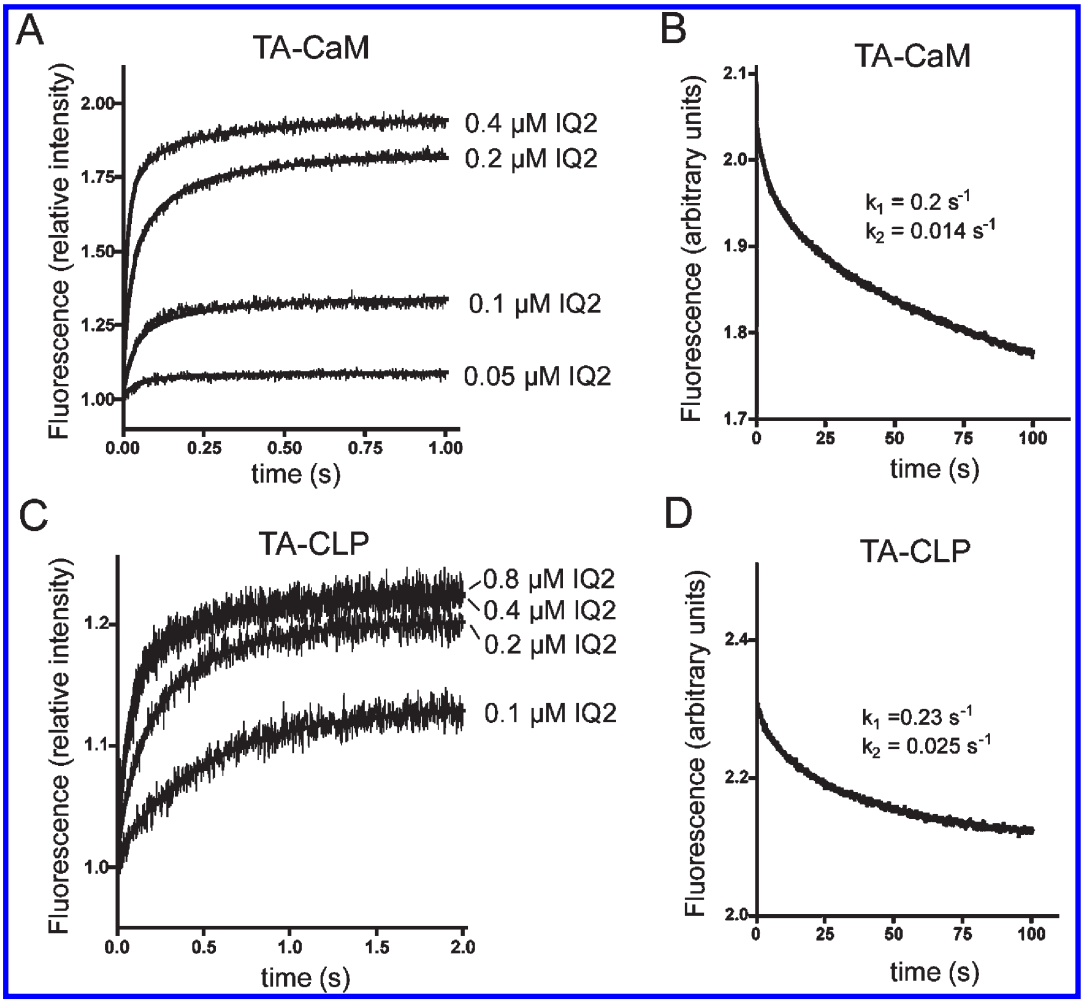

FIGURE 8: Kinetics of binding of TA-CaM and TA-CLP to IQ2 in the presence of 100 μM free Ca^{2+}. (A, C) Time course of fluorescence changes upon mixing 17 nM TA-CaM (A) or 17 nM TA-CLP (C) with the indicated concentrations of IQ2. The experimental data were fitted (smooth black lines) with the models and kinetic constants shown in Table 2. (B, D) Progress curves of the dissociation of TA-CaM (B) or TA-CLP (D) from IQ2. 34 nM TA-CaM or 34 nM TA-CLP was premixed with 0.2 μM IQ2, and dissociation was started by adding 1 μM CaM (B) or 1 μM CLP (D). The progress curves were fitted with a sum of two exponentials, with the constants shown in the figure. All media contained 0.2 mM EGTA and enough $CaCl_2$ to obtain 100 μM Ca^{2+}. In all cases, the indicated concentrations are after final mixing.

DISCUSSION

The purpose of this work was to establish kinetic parameters for the binding of the two known light chains of Myo10, CaM and CLP, to each of the IQ motifs in this myosin. To independently assess binding, we performed nondenaturing gels that allowed us to identify the complexes of IQ peptides with either CaM or CLP. The complexes were only detected in the presence of Ca^{2+}, suggesting that both CaM and CLP bind the individual IQ motifs with higher affinity in the Ca^{2+}-bound holo form. These qualitative assays also showed that, in an equimolar ratio, CLP was able to partially displace CaM from its complex with the IQ motifs and appeared to be most effective at competing with CaM for IQ2 and IQ3. Thus, it is likely that CLP, which is expressed only in specific tissues, can displace CaM from Myo10 in vivo, especially because CaM levels are thought to be limiting in cells (*22*).

To obtain quantitative information on the individual binding affinities of CaM and CLP for each IQ motif of Myo10, equilibrium titrations were performed with TA-CaM and TA-CLP. One observation that was initially unexpected (but is in agreement with the native gel electrophoresis data on complex formation) is that, in general, Ca^{2+} increased the affinity of both TA-CaM and TA-CLP for each of the IQ motifs. This was more evident for IQ1 and IQ3 than for IQ2 (see Table 1). In the presence of 100 μM Ca^{2+}, the affinity of TA-CaM and TA-CLP for IQ1 was between 30 and 100 times higher than in the absence of Ca^{2+}, yielding K_d values of ~50−150 nM. A high concentration of Ca^{2+} (100 μM) was chosen to saturate all four Ca^{2+} binding sites in both CaM and CLP; thus the (+Ca^{2+}) values reported in Table 1 reflect the affinity of the fully Ca^{2+}-loaded light chain for the specific IQ motif. The difference in the affinity in the absence and presence of Ca^{2+} is even more pronounced for the binding of TA-CaM and TA-CLP to IQ3. In the presence of Ca^{2+}, the affinity is very high (K_d values between 5 and 10 nM), whereas binding in the absence of Ca^{2+} was virtually undetectable. The effect of Ca^{2+} on the affinity of TA-CaM and TA-CLP for IQ2 is more modest, but still significant.

IQ motifs were initially thought to be preferred binding sites for (Ca^{2+}-free) apo-CaM (*9*, *10*). However, more recently it has been shown that this is not always the case and depends strongly on the sequence context of the IQ motifs and whether they are arranged in tandem (*23*, *24*). Martin and Bayley (*25*) showed that Ca^{2+} increases the affinity for CaM of a tandem made of IQ motifs 3 and 4 of MyoV. The data were interpreted to indicate that in the presence of Ca^{2+} CaM forms a bridge between contiguous IQ motifs with high affinity (*26*). A recent study on the IQ domain of Myo1c (a myosin-I family member) also found

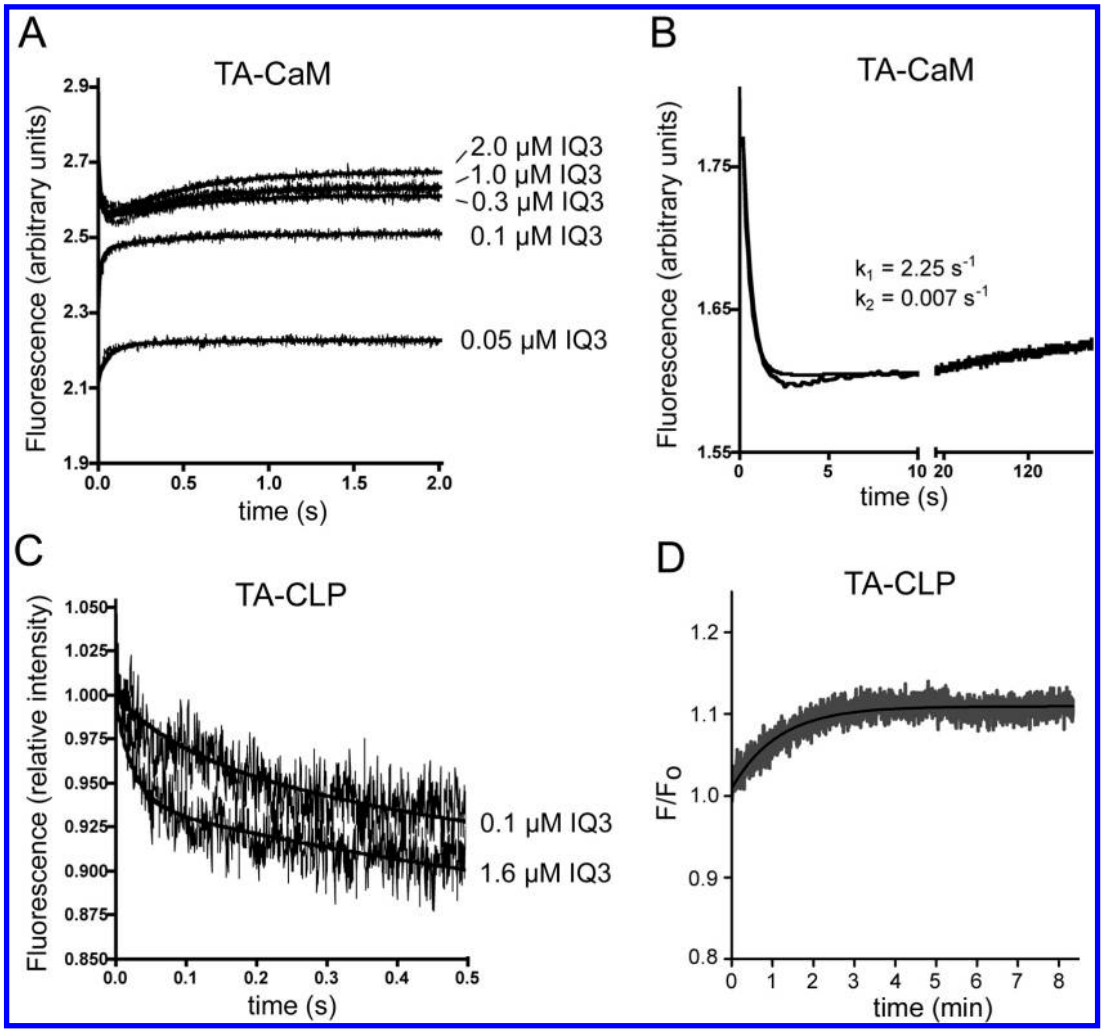

FIGURE 9: Kinetics of binding of TA-CaM and TA-CLP to IQ3 in the presence of 100 μM free Ca^{2+}. (A, C) Time course of fluorescence changes upon mixing 17 nM TA-CaM (A) or 17 nM TA-CLP (C) with the indicated concentrations of IQ3. In panel C, the data obtained with 0.2, 0.4, and 0.8 μM IQ3 were omitted from the figure for the sake of clarity, but the accuracy of the fit was comparable to that shown in the figure. The experimental data were fitted (smooth black line) with the models and kinetic constants shown in Table 2. (B, D) Time course of the dissociation of TA-CaM (B) or TA-CLP (D) from IQ3. 34 nM TA-CaM or 34 nM TA-CLP was premixed with 0.2 μM IQ3, and dissociation was started by adding 1 μM CaM (B) or 1 μM CLP (D). In panel B, the progress curve could be fitted with a sum of two exponentials, with the constants indicated in the figure. In contrast, dissociation of IQ3 from TA-CLP is slower ($k = 0.015\ s^{-1}$) and results in an increase of fluorescence (panel D). All media contained 0.2 mM EGTA and enough $CaCl_2$ to obtain 100 μM Ca^{2+}. In all cases, the indicated concentrations are after final mixing.

that CaM bound tightly to the tandem IQ motifs in both the presence and absence of Ca^{2+} (*27*). In addition, it has been pointed out that if IQ motifs have hydrophobic residues at positions 1−5−8−14 (as is typically found in Ca^{2+}-dependent CaM binding motifs), they may show Ca^{2+} dependency as well (*23*). All three IQ motifs of Myo10 do have hydrophobic residues in these positions (Figure 1), except for a Gln residue in position 8 of IQ3. It may be of interest in future studies to determine if and how changes in these hydrophobic residues affect the Ca^{2+} sensitivity of CaM and CLP binding to the Myo10 IQ motifs.

An interesting observation obtained from the stopped-flow experiments is that Ca^{2+} has very little effect on the rate of dissociation of either TA-CaM or TA-CLP from IQ1 and IQ2. By contrast, the rate constants derived from the kinetic analysis indicate that the forward reactions are faster in the presence of Ca^{2+}. In particular, Ca^{2+} increases the rate constant k_1 for the association of CaM with IQ1 and of CLP with IQ2, as well as the rate (k_5) of binding a second IQ peptide by CaM and CLP (see Table 2). These results suggest that CaM and CLP could be prone to forming "bridges" between different (adjacent) tandem IQs in Myo10 in the presence of Ca^{2+}. The results are in keeping with the findings of Martin and Bayley (*26*), who reported the formation of very high affinity 1:1 complexes of CaM with tandem IQ motifs from MyoV in the presence of Ca^{2+}. It should be noted, however, that our experiments showed that binding of a second IQ peptide to CaM or CLP required the peptide to be in large excess, suggesting the low affinity of such a possible second binding event.

IQ3 shows very different kinetic characteristics when compared to IQ1 and IQ2: (i) For both TA-CaM and TA-CLP, there is little or no binding in the absence of Ca^{2+}. (ii) Binding of TA-CaM to IQ3 shows an overall increase in fluorescence, while binding of TA-CLP shows a decrease in fluorescence. By contrast, both TA-CaM and TA-CLP show a similar pattern of overall fluorescence change upon binding to IQ1 or IQ2. (iii) The progress curve of TA-CaM binding to IQ3 shows a very complex multistep pattern, whereas the mechanism of TA-CLP binding to IQ3 seems much simpler (compare model 5 with model 2 in Figure 4). We emphasize that the binding schemes in Table 2 must be interpreted with caution, as these are merely models

yielding optimal fits of the experimental data. The exact chemical nature of the intermediate steps is undetermined; thus definite conclusions as to the structure and conformation of different TA-CaM or TA-CLP complexes with a single or two IQ peptides must await high-resolution structural determination. However, regardless of the uncertainties associated with the precise structures of the complexes, the binding of TA-CLP to IQ3 follows a very different kinetic path compared to TA-CaM.

Multiple effects contribute to the fluorescence changes induced by binding of the IQ peptides to TA-CaM or TA-CLP. These include conformational changes of TA-CaM/TA-CLP upon interaction with the peptides, as well as possible changes in the fluorescence yield of the complexes caused by induced secondary structure stabilization of the IQ peptides upon binding. Therefore, the structural identity of the kinetic intermediates postulated by the models (such as TA-C−IQ* and TA-C−IQ^) remains undetermined. However, the distinct kinetic steps likely correspond to major structural transitions in TA-CaM/TA-CLP and/or the peptide(s), which affect the environment of the fluorescent TA moiety.

When discussing the kinetic differences in light chain binding to these IQ motifs, it is important to keep their sequence differences in mind. None of these IQ motifs comply with all the characteristics of the canonical IQ motif IQxxxRGxxxR. IQ1 contains an R residue instead of a Q in the initial IQ, and the RG is changed to LG. Although an R at position 2 in this motif can participate in a network of H-bonds like Q does, it is a charged and more bulky residue, potentially rationalizing why IQ1 has lower affinity for the light chain than IQ2 and IQ3. IQ2 is close to the canonical sequence, the only modification being RA instead of RG. The effect of substitution of the canonical G by A in this position has recently been studied in a reference IQ motif and was found to decrease the affinity for CaM in the absence of Ca^{2+} but increase the affinity for Ca^{2+}-bound CaM (*28*). However, of the three Myo10 IQs, IQ2 still has the highest affinity for both Ca^{2+}-free CLP and CaM (Table 1), suggesting that other residues within the IQ motif are equally important for binding to CaM and CLP in the absence of Ca^{2+}. Finally, in IQ3, the aliphatic I in position 1 is replaced by F (a bulky aromatic residue). Whether this replacement is sufficient to confer the observed different properties to IQ3 in regard to the effect of Ca^{2+} on light chain binding remains to be addressed in future work. However, it is interesting to note that an F > A mutation in IQ3 drastically reduced CLP, but not CaM, binding (*29*).

A pending question concerns the changes that will occur in terms of light chain binding to the IQ1−3 neck region of Myo10 upon a rise in Ca^{2+}. Given the complexity of the issue, one can only speculate at this point. However, in light of our results some general points may be legitimate: (a) binding of both CaM and CLP is expected to increase with a rise of Ca^{2+}; (b) no significant change in the rate of dissociation of either CaM or CLP may occur, but rebinding could be impaired by one light chain forming a tight bridge between neighboring IQ motifs, especially between IQ1 and IQ2; (c) regarding which light chain would prevail, in the "in vitro" conditions CaM and CLP show comparable affinities. However, "in vivo" the conditions might differ, considering that CaM has many more targets than CLP. Therefore, its free concentration in the cell is greatly reduced (*22*). Binding to the full-length Myo10, with its three IQ motifs in tandem, might pose additional restrictions and properties not seen when studying binding to isolated IQ motifs. Therefore, drawing conclusions as to which light chain will prevail *in vivo* is premature at this point and beyond the scope of this paper.

ACKNOWLEDGMENT

We thank Dr. Katalin Török (St. Geoge Hospital Medical School, London, U.K.) and Dr. Richard Thorogate (London Centre for Nanotechnology, University College London, U.K.) for the generous gift of TA-CaM and TA-CLP.

REFERENCES

1. Berg, J. S., Derfler, B. H., Pennisi, C. M., Corey, D. P., and Cheney, R. E. (2000) Myosin-X, a novel myosin with pleckstrin homology domains, associates with regions of dynamic actin. *J. Cell Sci. 113*, 3439–3451.
2. Berg, J. S., and Cheney, R. E. (2002) Myosin-X is an unconventional myosin that undergoes intrafilopodial motility. *Nat. Cell Biol. 4*, 246–250.
3. Toyoshima, F., and Nishida, E. (2007) Integrin-mediated adhesion orients the spindle parallel to the substratum in an EB1- and myosin X-dependent manner. *EMBO J. 26*, 1487–1498.
4. Woolner, S., O'Brien, L. L., Wiese, C., and Bement, W. M. (2008) Myosin-10 and actin filaments are essential for mitotic spindle formation. *J. Cell Biol. 182*, 77–88.
5. Yonezawa, S., Yoshizaki, N., Sano, M., Hanai, A., Masaki, S., Takizawa, T., Kageyama, T., and Moriyama, A. (2003) Possible involvement of myosin-X in intercellular adhesion: importance of serial pleckstrin homology regions for intracellular localization. *Dev., Growth Differ. 45*, 175–185.
6. Zhang, H., Berg, J. S., Li, Z., Wang, Y., Lang, P., Sousa, A. D., Bhaskar, A., Cheney, R. E., and Strömblad, S. (2004) Myosin-X provides a motor-based link between integrins and the cytoskeleton. *Nat. Cell Biol. 6*, 523–531.
7. Berg, J. S., Powell, B. C., and Cheney, R. E. (2001) A millennial myosin census. *Mol. Biol. Cell 12*, 780–794.
8. Krendel, M., and Mooseker, M. S. (2005) Myosins: tails (and heads) of functional diversity. *Physiology 20*, 239–251.
9. Cheney, R. E., and Mooseker, M. S. (1992) Unconventional myosins. *Curr. Opin. Cell Biol. 4*, 27–35.
10. Wolenski, J. S. (1995) Regulation of calmodulin-binding myosins. *Trends Cell Biol. 5*, 310–316.
11. Homma, K., Saito, J., Ikebe, R., and Ikebe, M. (2001) Motor function and regulation of myosin X. *J. Biol. Chem. 276*, 34348–34354.
12. Rogers, M. S., and Strehler, E. E. (2001) The tumor-sensitive calmodulin-like protein is a specific light chain of human unconventional myosin X. *J. Biol. Chem. 276*, 12182–12189.
13. Bennett, R. D., Mauer, A. S., and Strehler, E. E. (2007) Calmodulin-like protein increases filopodia-dependent cell motility via up-regulation of myosin-10. *J. Biol. Chem. 282*, 3205–3212.
14. Durussel, I., Rhyner, J. A., Strehler, E. E., and Cox, J. A. (1993) Cation binding and conformation of human calmodulin-like protein. *Biochemistry 32*, 6089–6094.
15. Rhyner, J. A., Koller, M., Durussel-Gerber, I., Cox, J. A., and Strehler, E. E. (1992) Characterization of the human calmodulin-like protein expressed in *Escherichia coli*. *Biochemistry 31*, 12826–12832.
16. Qian, H., Rogers, M. S., Schleucher, J., Edlund, U., Strehler, E. E., and Sethson, I. (1998) Sequential assignment of ^{1}H, ^{15}N, ^{13}C resonances and secondary structure of human calmodulin-like protein determined by NMR spectroscopy. *Protein Sci. 7*, 2421–2430.
17. Török, K., and Trentham, D. R. (1994) Mechanism of 2-chloro-(ε-amino-Lys75)-[6-[4-(N,N-diethylamino)phenyl]-1,3,5-triazin-4-yl]-calmodulin interactions with smooth muscle myosin light chain kinase and derived peptides. *Biochemistry 33*, 12807–12820.
18. Penheiter, A. R., Bajzer, Z., Filoteo, A. G., Thorogate, R., Török, K., and Caride, A. J. (2003) A model for the activation of plasma membrane calcium pump isoform 4b by calmodulin. *Biochemistry 42*, 12115–12124.
19. Akaike, H. (1974) A new look at the statistical model identification. *IEEE Trans. Autom. Control 19*, 716–723.
20. Penheiter, A. R., Filoteo, A. G., Penniston, J. T., and Caride, A. J. (2005) Kinetic analysis of the calmodulin-binding region of the plasma membrane calcium pump isoform 4b. *Biochemistry 44*, 2009–2020.
21. Caride, A. J., Filoteo, A. G., Penniston, J. T., and Strehler, E. E. (2007) The plasma membrane Ca^{2+} pump isoform 4a differs from isoform 4b in the mechanism of calmodulin binding and activation kinetics. *J. Biol. Chem. 282*, 25640–25648.
22. Persechini, A., and Stemmer, P. M. (2002) Calmodulin is a limiting factor in the cell. *Trends Cardiovasc. Med. 12*, 32–37.
23. Bähler, M., and Rhoads, A. (2002) Calmodulin signaling via the IQ motif. *FEBS Lett. 513*, 107–113.

24. Li, Z., and Sacks, D. B. (2003) Elucidation of the interaction of calmodulin with the IQ motifs of IQGAP1. *J. Biol. Chem. 278*, 4347–4352.
25. Martin, S. R., and Bayley, P. M. (2002) Regulatory implications of a novel mode of interaction of calmodulin with a double IQ-motif target sequence from murine *dilute* myosin V. *Protein Sci. 11*, 2909–2923.
26. Martin, S. R., and Bayley, P. M. (2004) Calmodulin bridging of IQ motifs in myosin-V. *FEBS Lett. 567*, 166–170.
27. Manceva, S., Lin, T., Pham, H., Lewis, J. H., Goldman, Y. E., and Ostap, E. M. (2007) Calcium regulation of calmodulin binding to and dissociation from the Myo1c regulatory domain. *Biochemistry 46*, 11718–11726.
28. Black, D. J., and Persechini, A. (2010) Variations at the semiconserved glycine in the IQ domain consensus sequence have a major impact on Ca^{2+}-dependent switching in calmodulin-IQ domain complexes. *Biochemistry 49*, 78–83.
29. Bennett, R. D., Caride, A. J., Mauer, A. S., and Strehler, E. E. (2008) Interaction with the IQ3 motif of myosin-10 is required for calmodulin-like protein-dependent filopodial extension. *FEBS Lett. 582*, 2377–2381.